Appendix to:

Legendre P, Gauthier O. 2014 Statistical methods for temporal and space-time analysis of community composition data. *Proc. R. Soc. B* **281**, xxx–xxx.

Appendix S3

Figures from the Practicals in R

This appendix contains the figures produced during the Practical exercises of Appendix S2 that are not included in the paper. In addition, Figure S3.1, referred to in the main paper, is presented in this appendix.

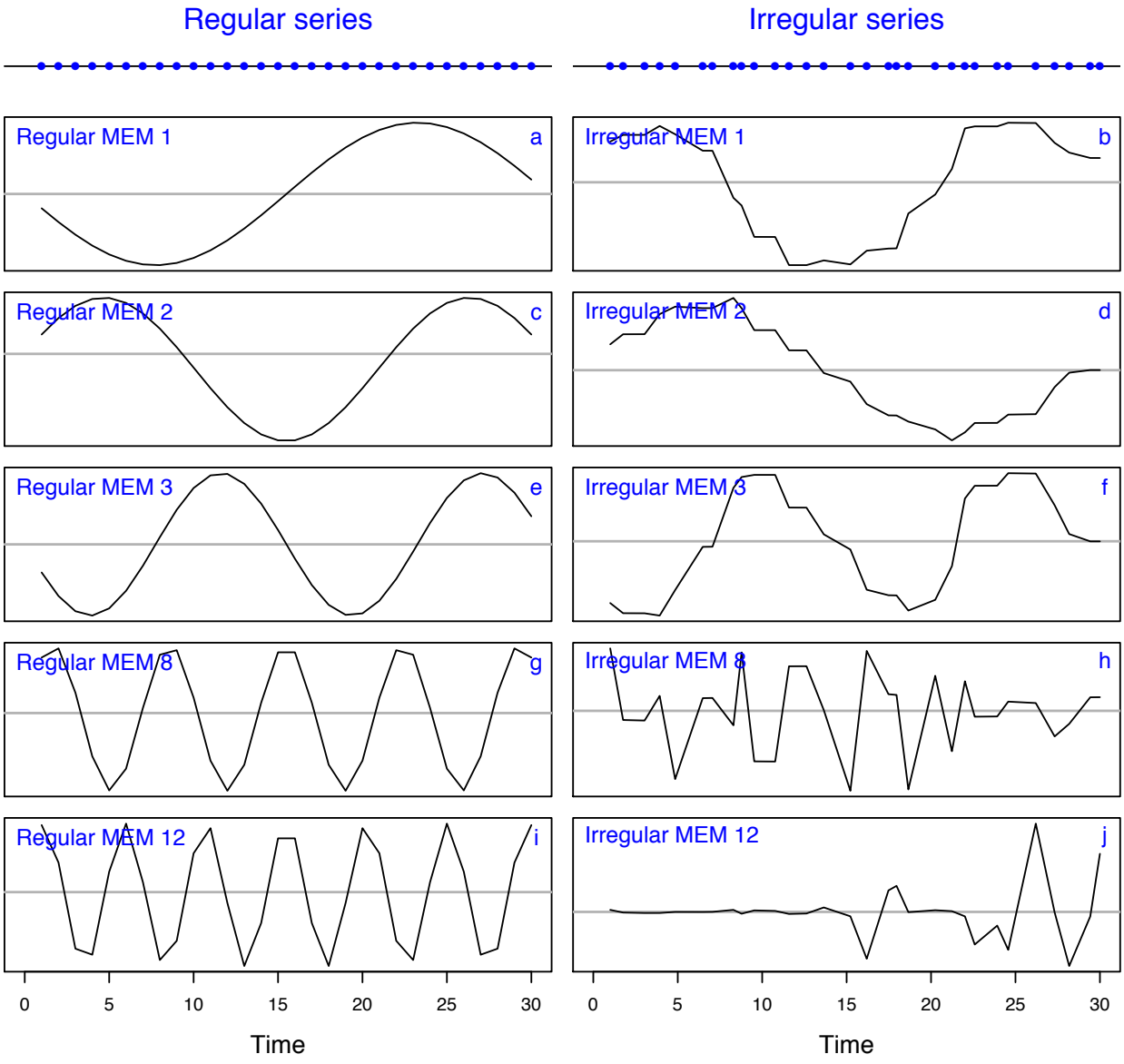

Figure S3.1. A selection of dbMEM eigenfunctions computed for a series of 30 observations. Left: regularly-spaced observations, truncation distance = 1. Right: irregularly-spaced observations, truncation distance = 1.6. In each case, there were 29 eigenfunctions in total, 14 of which modelled positive temporal correlation. As the irregularity of the observations along the series increases, there may be fewer functions modelling positive temporal correlation, and the non-stationary character of the last ones increases. Hence a regular sampling design may produce models with higher R^2 and tests with more power. Top: position of the observations in each series. See Blanchet *et al*. (2011, Fig. E1 and E2) for similar pictures drawn for 100 points.

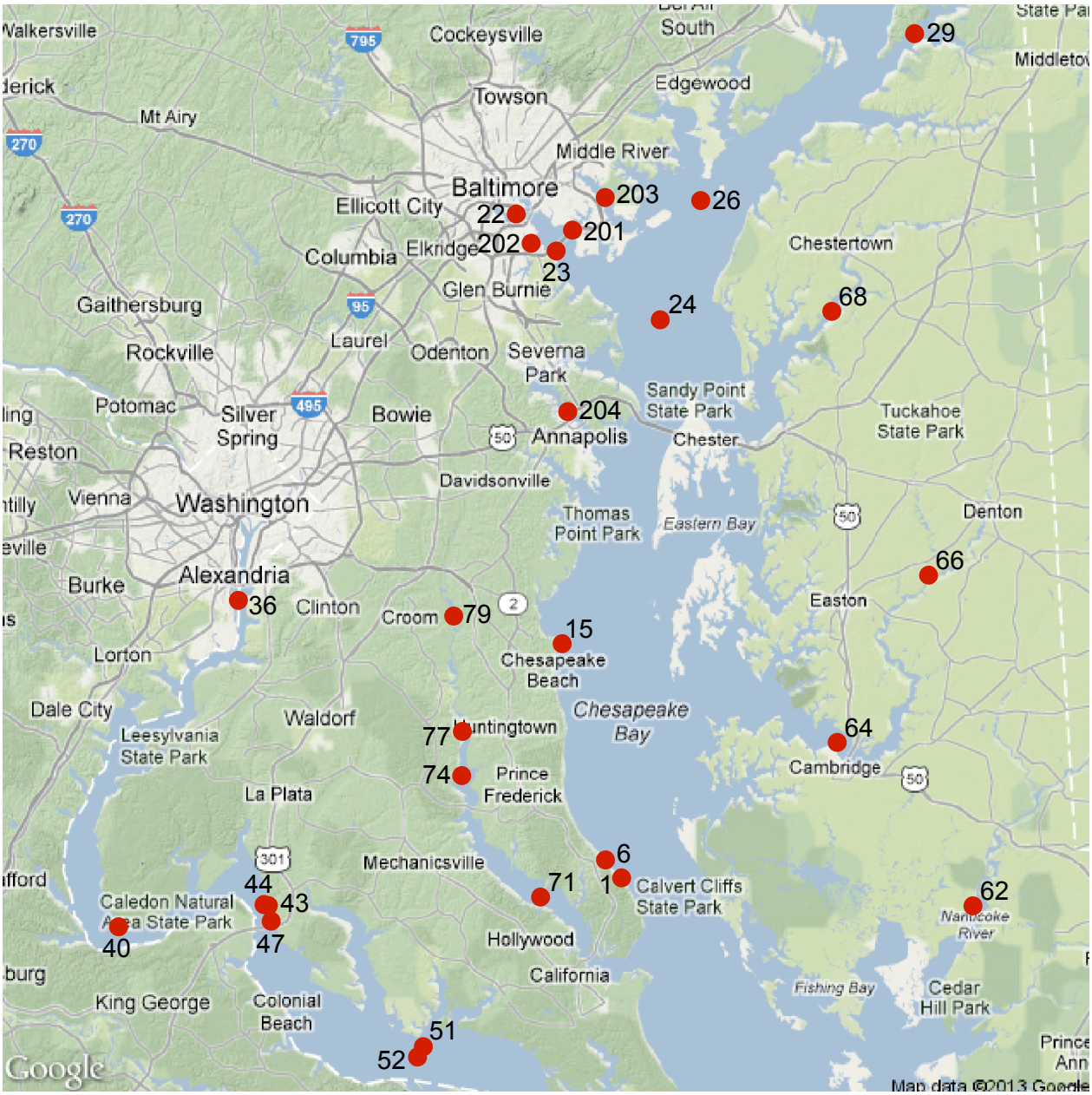

Figure S3.2. Map of the 27 Chesapeake Bay ecological survey fixed sampling sites.

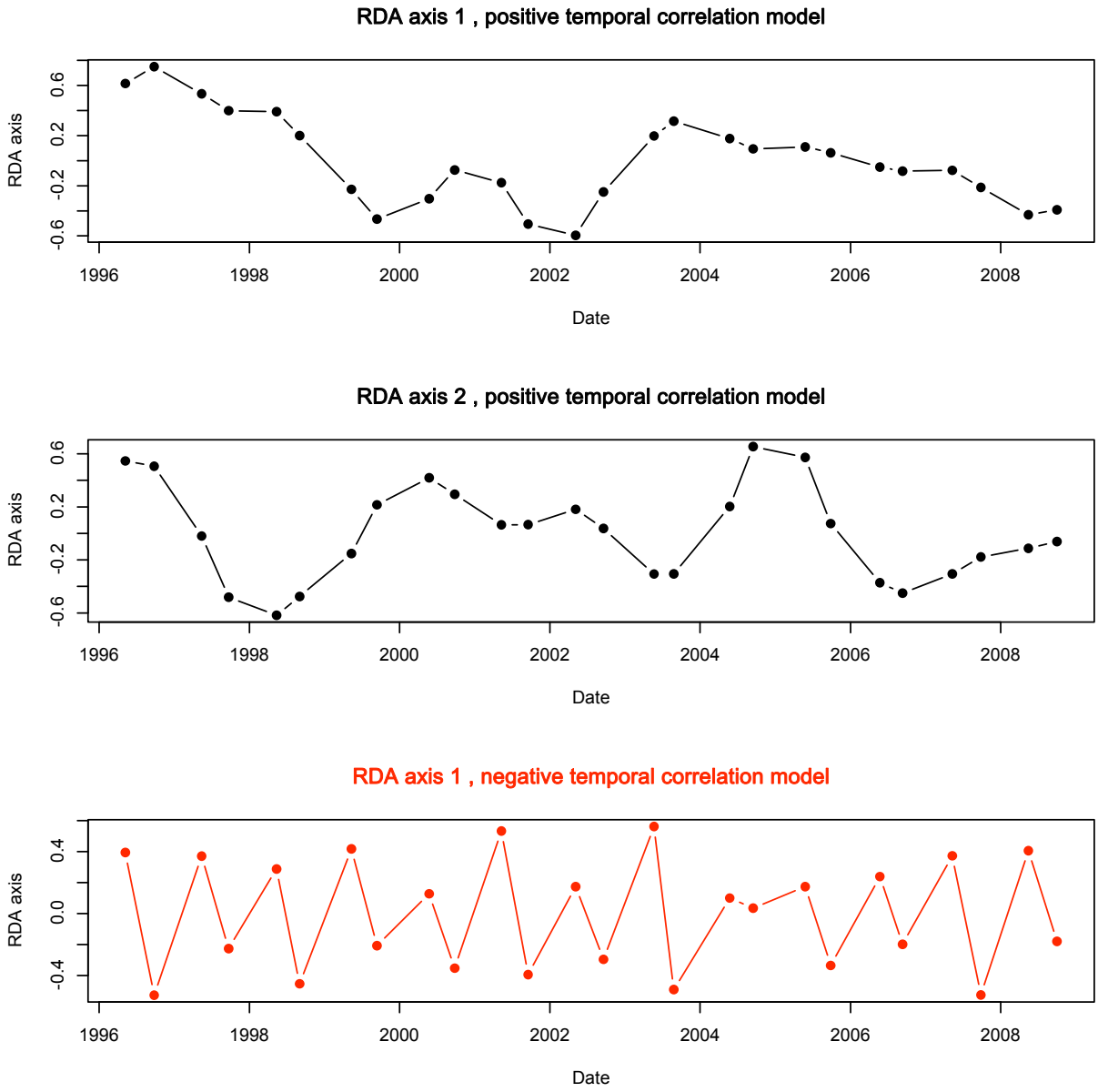

Figure S3.3. Temporal variation of values along the significant ($p < 0.05$) canonical axes of dbMEM models of the site 40 Hellinger-transformed macrofaunal data constructed using all positive (top and middle panels) and negative (bottom panel) dbMEM. Along the abscissa, year labels are shown on January 1st of the year.

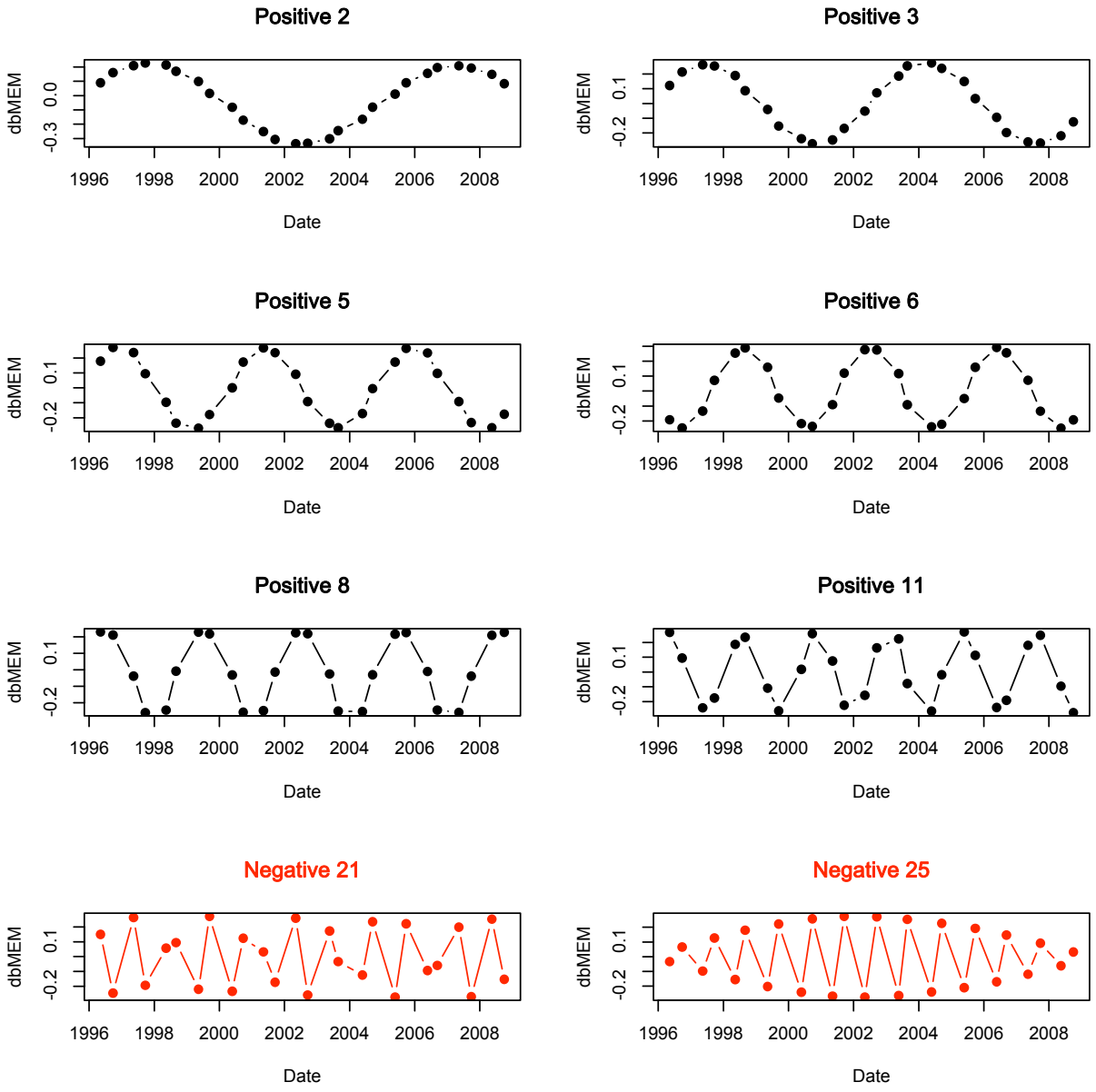

Figure S3.4. The 8 dbMEM eigenfunctions selected by forward selection ($p < 0.05$) from the pool of all available dbMEM for the site 40 data. dbMEM 2, 3, 5, 6, 8 and 11, which model positive temporal correlation, are plotted in black, while dbMEM 21 and 25, which correspond to negative temporal correlation, are plotted in red. Along the abscissa, year labels are shown on January 1st of the year. Note that the signs of the eigenfunctions may be inverted when the calculations are done on different computers or using different software; that is of no consequence.

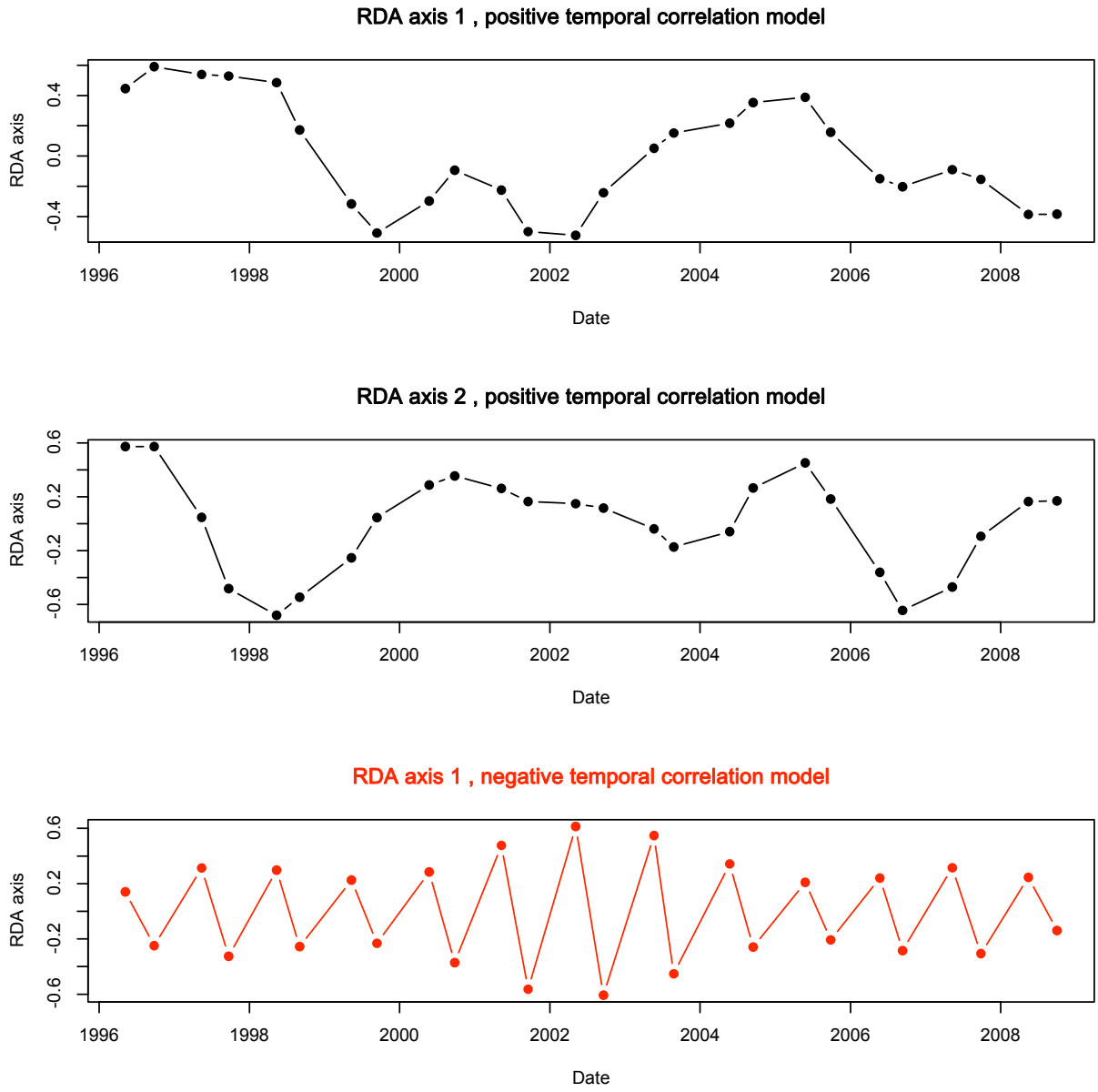

Figure S3.5. Temporal variation of values along the significant ($p < 0.05$) canonical axes of dbMEM models of the Hellinger-transformed site 40 macrofaunal data constructed using forward-selected positive (top and middle panels) and negative (bottom panel) dbMEM. Along the abscissa, year labels are shown on January 1st of the year. dbMEM were selected at the 0.05 level.

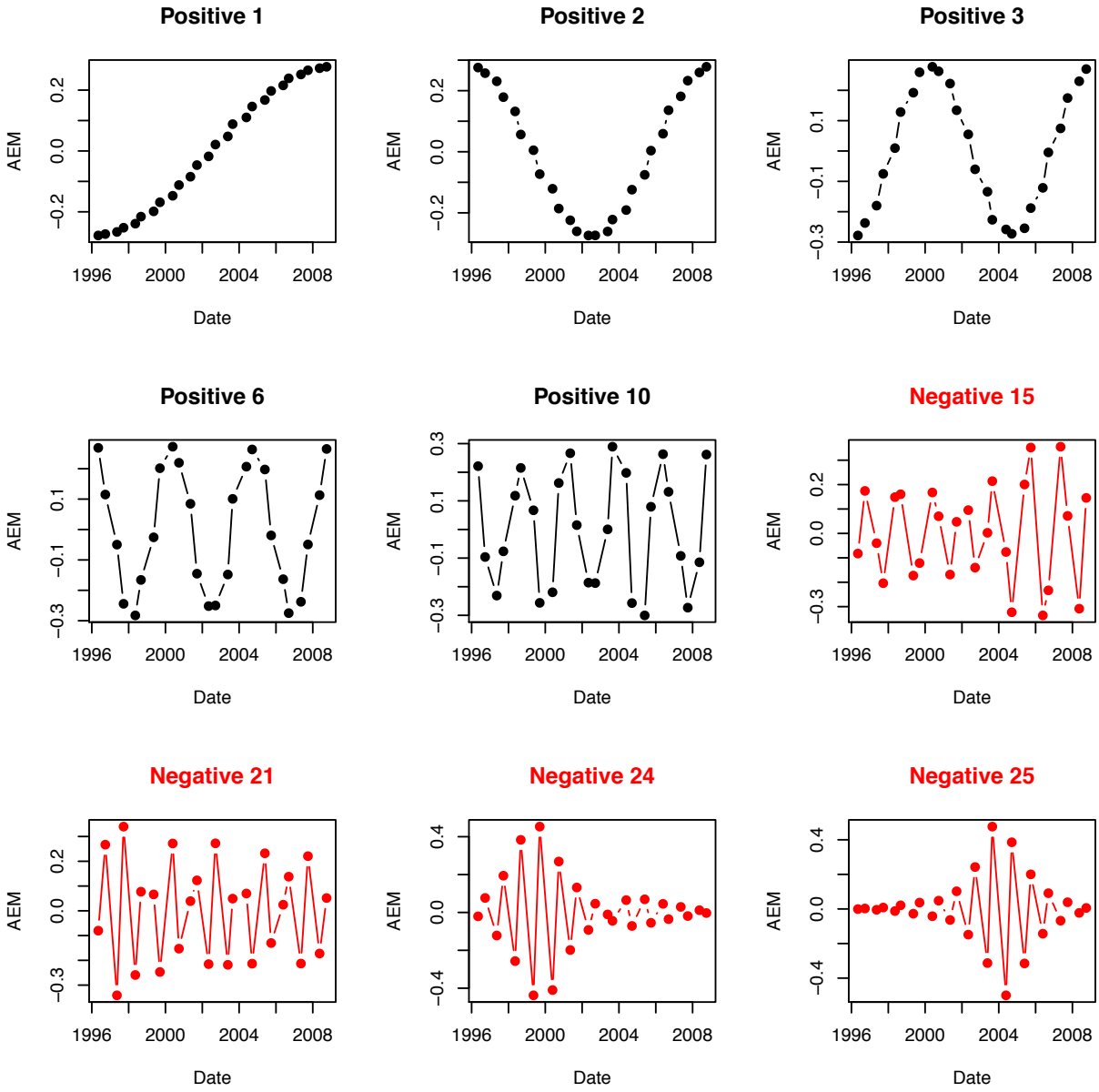

Figure S3.6. The 9 AEM selected by forward selection ($p < 0.08$) from the pool of all available AEM for the site 40 data. AEM 1, 2, 3, 6 and 10, which model positive temporal correlation, are plotted in black, while AEM 15, 21, 24 and 25, which correspond to negative temporal correlation, are plotted in red. Along the abscissa, year labels are shown on January 1st of the year.

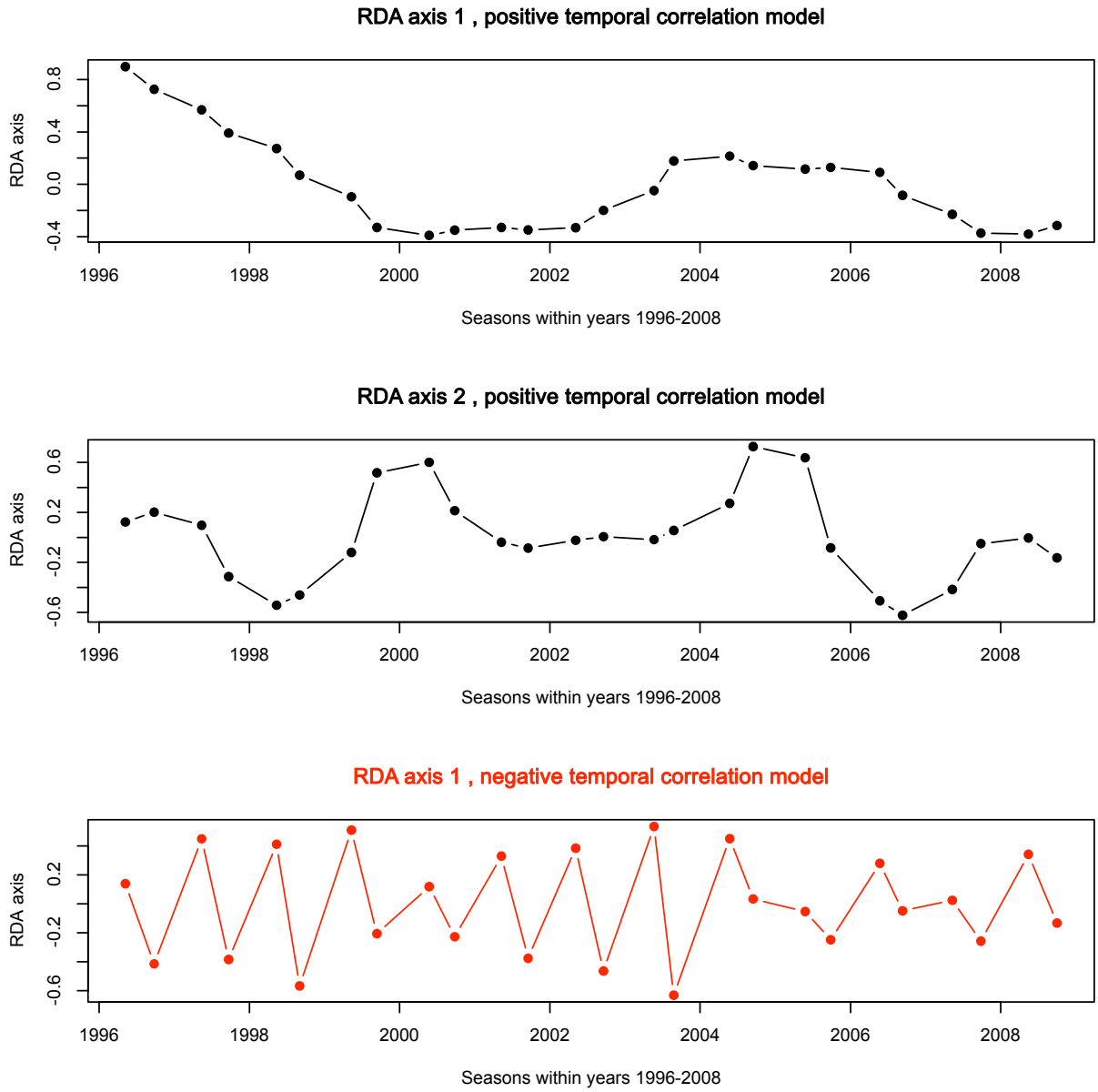

Figure S3.7. Temporal variation of values along the significant ($p < 0.05$) axes of canonical AEM models of the Hellinger-transformed site 40 macrofaunal data constructed using forward-selected positive (top and middle panels) and negative (bottom panel) AEM. Along the abscissa, year labels are shown on January 1st of the year. AEM were selected at the 0.08 level.

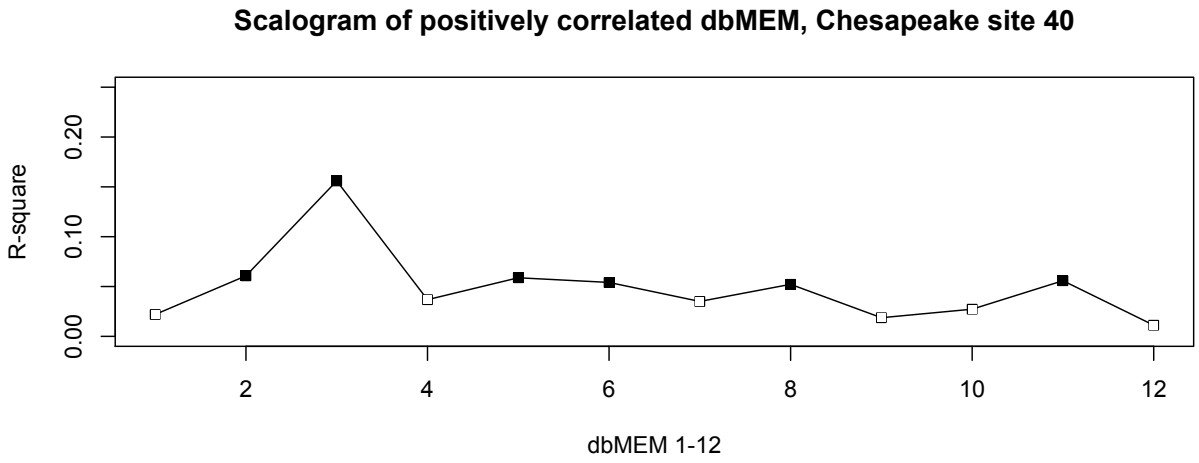

Figure S3.8. Scalogram of the 12 dbMEM modelling positive temporal correlation of the site 40 data. Values on the ordinate are semipartial R^2 computed separately for each dbMEM. The statistics of the dbMEM that were selected by forward selection (i.e. the six that significantly contributed to model the faunal response data; see Figure S3.3) are represented by black squares.

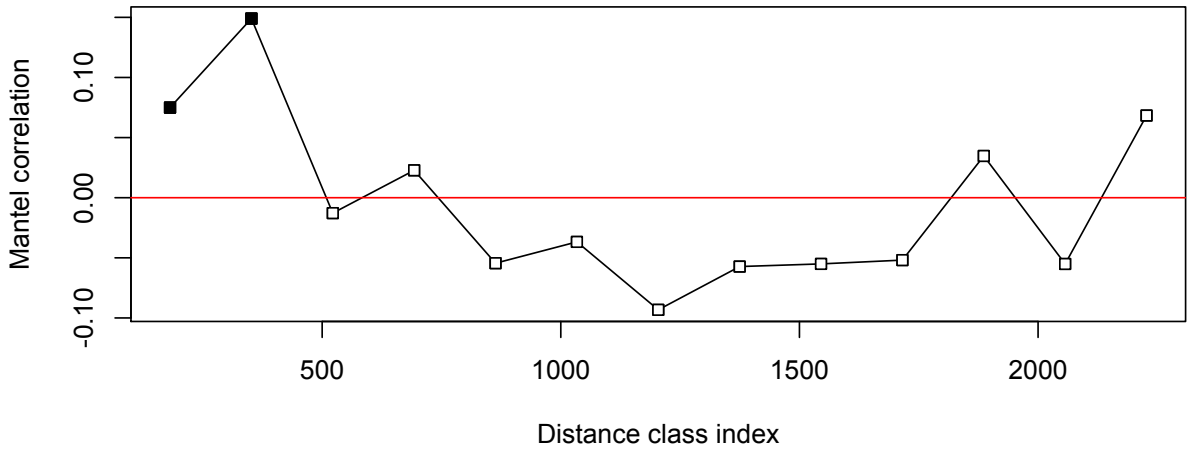

Figure S3.9. Multivariate Mantel correlogram of the site 40 Hellinger-transformed macrofaunal data. Maximum and significant positive correlation is found between observations in the second distance class, which corresponds to pairs of observations one year apart. Observations made in subsequent seasons are also, but somewhat less, positively correlated. Larger distance classes exhibit no significant temporal correlation.

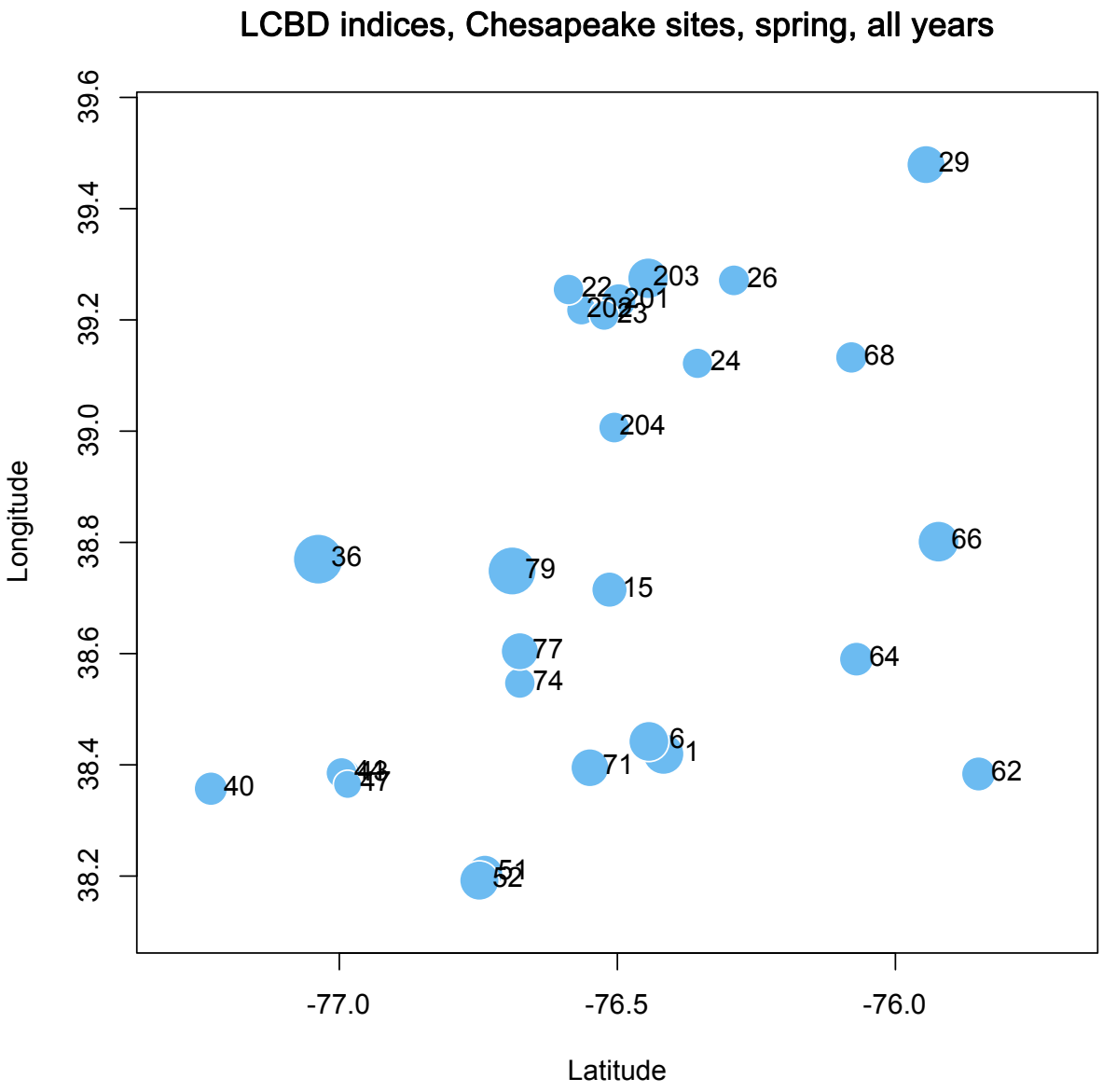

Figure S3.10. Map of LCBD values at the 27 sites, summed over the 13 years, for the spring surveys. The circle surface areas are proportional to the LCBD values.

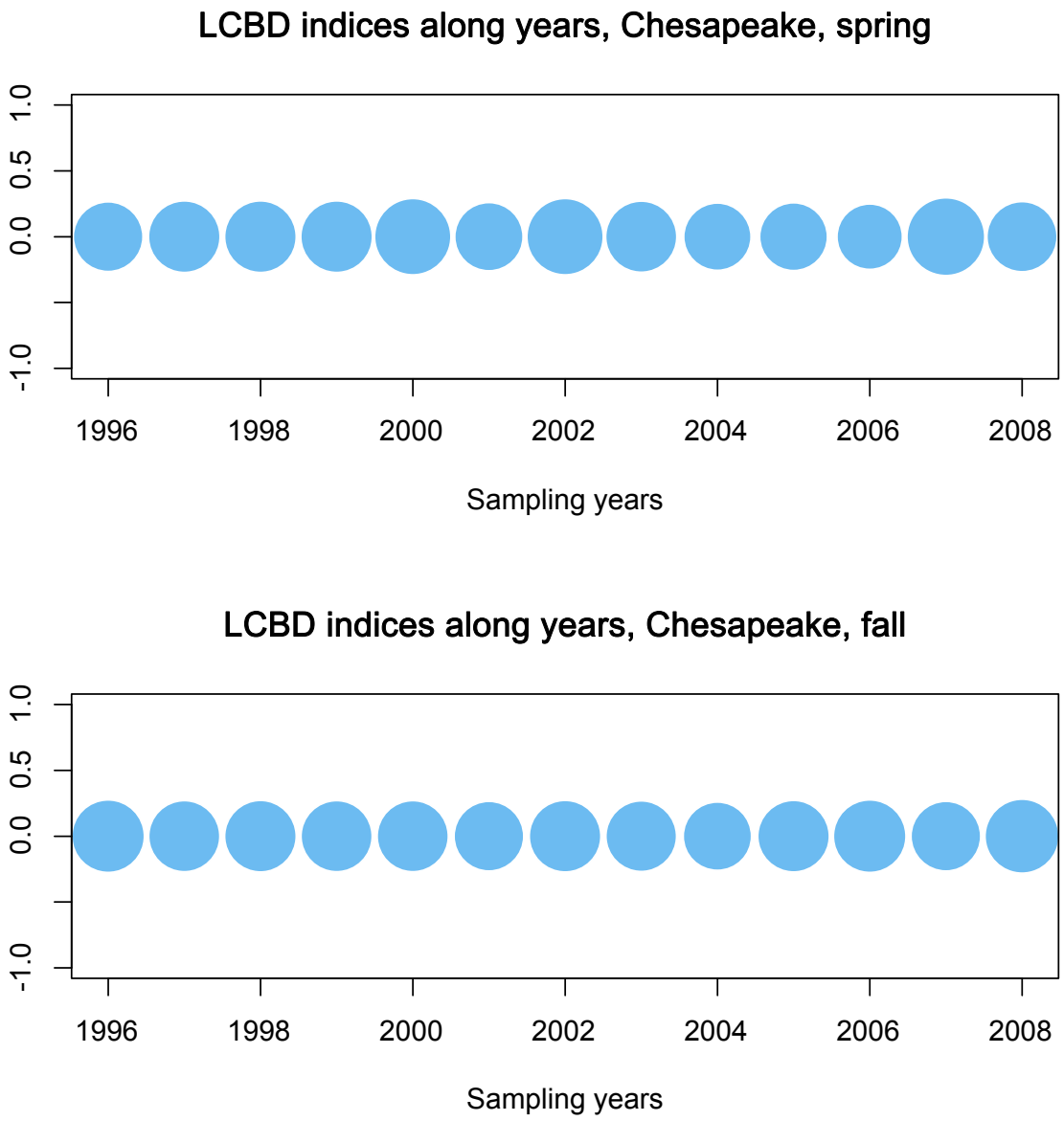

Figure S3.11. Time maps of LCBD values per year, summed over the sites, for the spring (top panel) and fall (bottom panel) surveys.

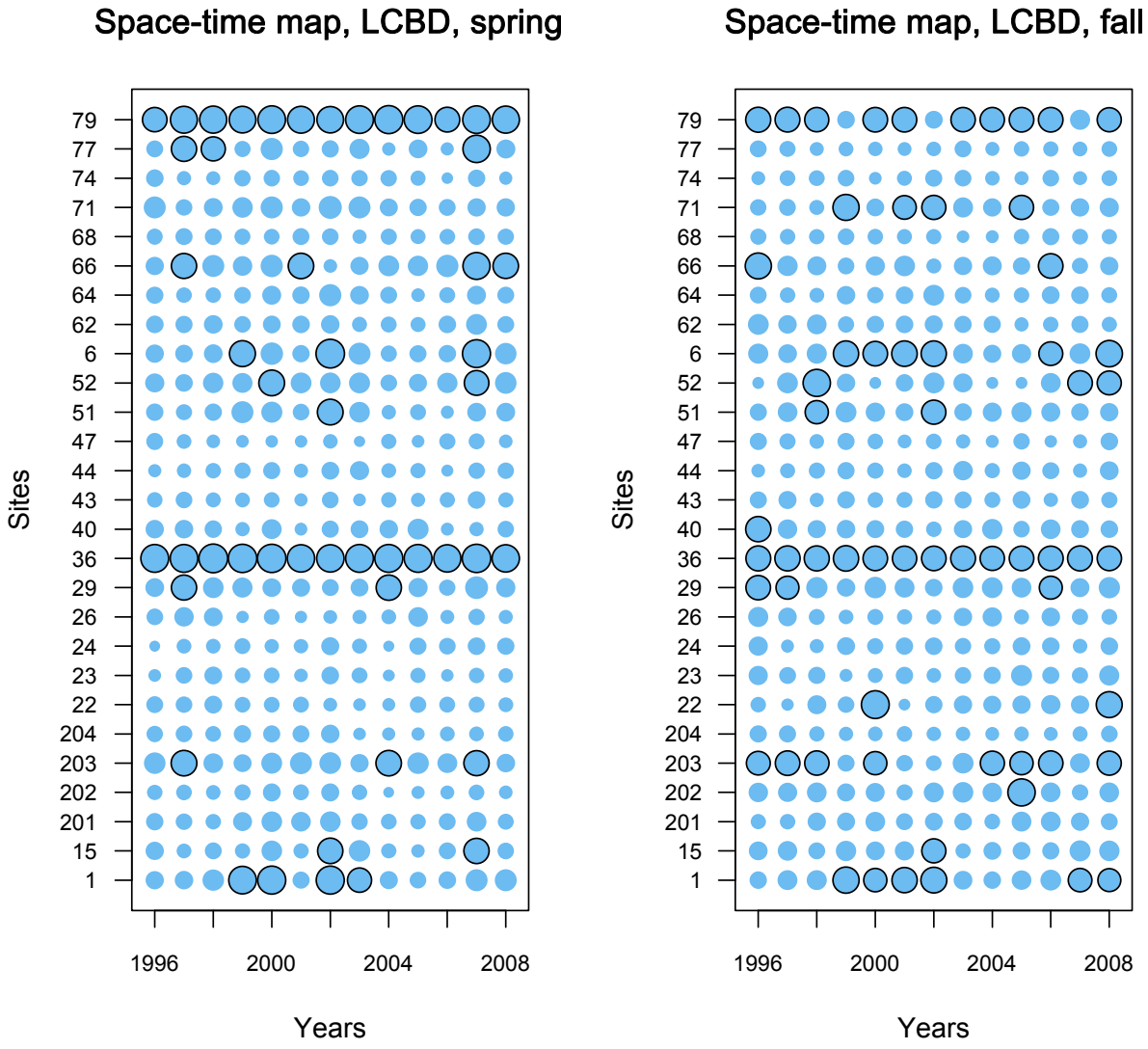

Figure S3.12. Space-time maps (27 sites, 13 years) of LCBD indices computed separately for the spring and fall data. The circle surface areas are proportional to the LCBD values. Circles with a black rim indicate significant LCBD values at the 0.05 level.

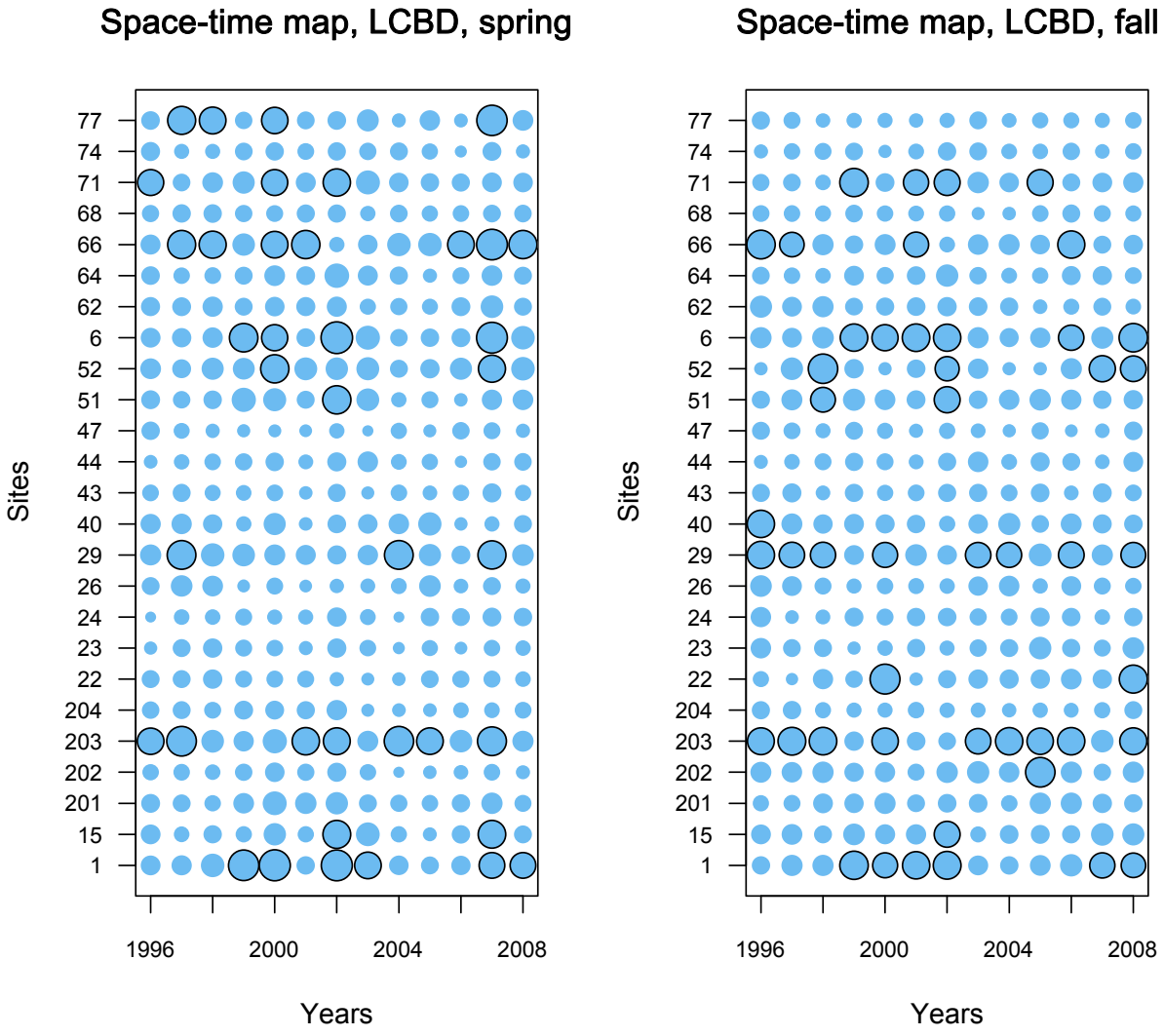

Figure S3.13. Space-time maps (25 sites, 13 years) of LCBD indices computed separately for the spring and fall data. Within each map, the surface area of the circles is proportional to the LCBD. Circles with a black rim indicate significant LCBD values at the 0.05 level.

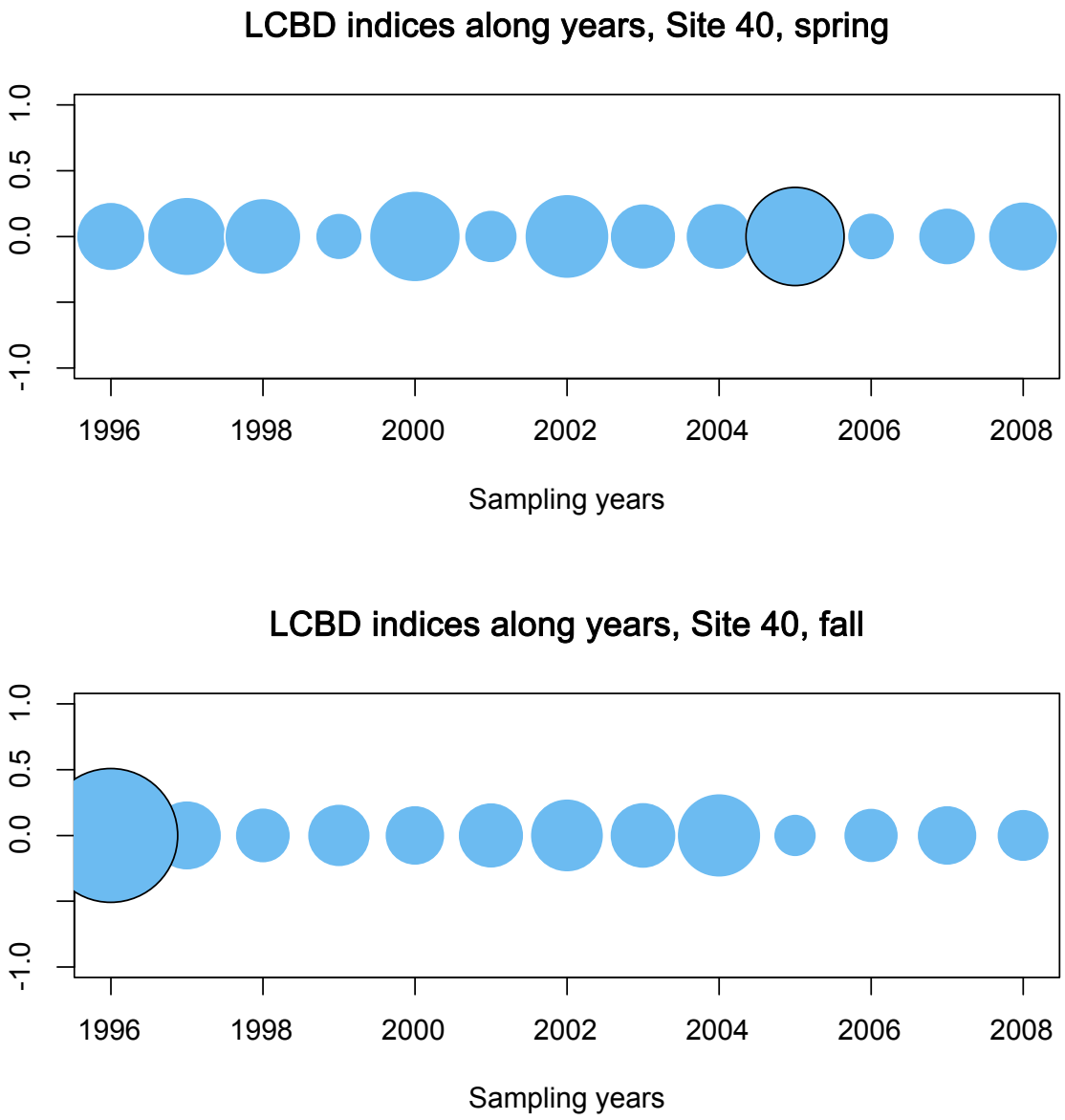

Figure S3.14. Time maps of LCBD values per year for the spring (top panel) and fall (bottom panel) surveys at site 40. Circles with a black rim indicate significant LCBD values at the 0.05 level.

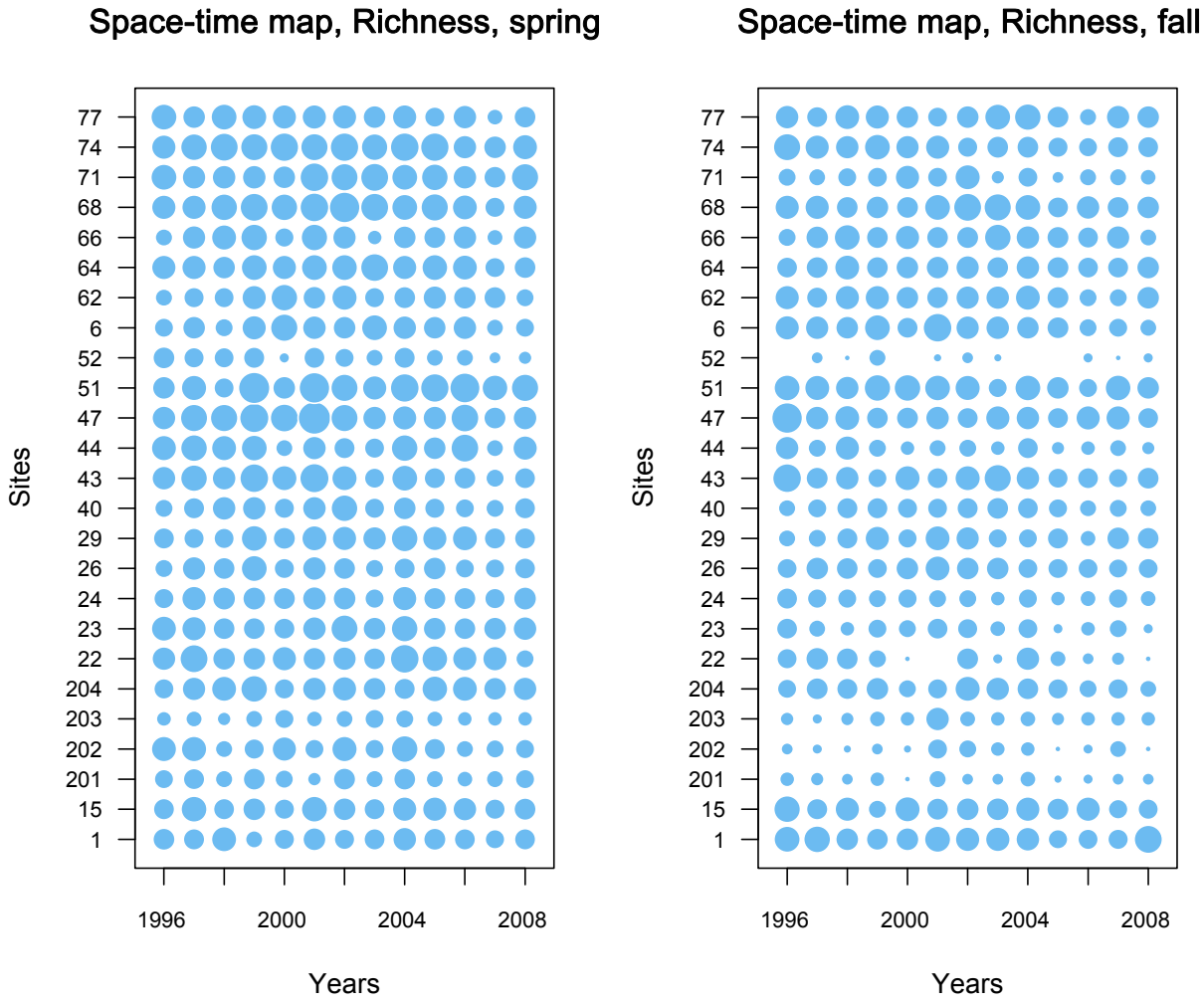

Figure S3.15. Space-time maps (25 sites, 13 years) of taxonomic richness computed separately for the spring and fall surveys.